THE EFFECT OF NON-METALLIC INCLUSIONS ON THE HOT DUCTILITY OF CONTINUOUSLY CAST LOW-ALLOY STEEL

C. I. Garcia*, S. Pytel*+, A. J. DeArdo*

Elevated and room temperature deformation tests were used to evaluate the hot ductility of a continuously cast low-alloy steel. Factors such as, temperature, amount of deformation, and non-metallic inclusion morphology were studied in terms of their influence on the fracture behavior of this steel. Quantitative fractographic studies were conducted to assess the mechanisms of crack growth and coalescence that occured in the vicinity of the non-metallic inclusions during the deformation of the steel tested.

INTRODUCTION

It is well known that the hot ductility of steels is strongly dependent on both the material properties and hot working processes (1-5). Some of the principal factors that influence the properties of the material are: alloy composition, phase and precipitation reactions, thermomechanical processing, structure and the cleanliness of the steel. Among these factors, the deleterious effect of non-metallic inclusions on the hot ductility of steels has been and continues to be a major concern. For example, the complex interaction between the composition, morphology and distribution of non-metallic inclusions, and hot workability parameters (e.g. temperature, strain, strain rate, etc.) is a very difficult relationship to assess. In previous years, tension and torsion tests have been two of the most widely used methods to measure the hot ductility of steels; however these techniques have their advantages and limitations, and have been discussed elsewhere (3-6). In recent years, Kuhn et. al (7) proposed a new procedure

* Basic Metals Processing Research Institute, affiliated with the Department of Materials Science and Engineering, University of Pittsburgh, Pittsburgh, PA 15261 U.S.A.
*+Technical University of Cracow M-2, 31-864 Krakow, Poland

to evaluate hot ductility. The purpose of this work is to present results of the hot ductility of a continuously cast low-alloy steel as a function of the morphology and distribution of non-metallic inclusions using Kuhn's method. In addition, results of the ductile fracture mechanisms in the low-alloy steel at high and room temperature are also presented.

THEORETICAL ASPECTS

It is generally accepted that the ductility of a steel can be influenced by changes in the volume fraction, distribution, shape and composition of non-metallic inclusions. Large numbers of studies concerning ductile fracture of alloys composed of a soft matrix and hard second phase particles have recognized that nucleation, growth and coalescence of microcracks take place during the deformation of these alloys. Concerning microcrack nucleation at second phase particles, several theoretical models have been proposed (8-9). However, these models are concerned with situations in which the second phase particles are much stronger bonded with the matrix. When the second phase particles are non-metallic inclusions (e.g. MnS), the aforementioned models are not completely acceptable. In the case of sulfide inclusions, a prevailing mechanism of crack nucleation is the void formation at the matrix-inclusion interface in early stages of plastic flow (10).

The second stage of ductile fracture (void growth) can be quantitatively described on the basis of the void growth ratio, υ, (10). The void growth ratio for a given volume fraction of non-metallic inclusions can be defined as follows:

$$\upsilon = \frac{d\varepsilon_1}{d\delta_1} \quad \ldots\ldots\ldots\ldots \quad (1)$$

If we assume that υ is constant, then equation (1) can be written

$$\upsilon = \frac{\varepsilon_1}{\delta_1} \quad \ldots\ldots\ldots\ldots \quad (2)$$

The strains ε_1 and δ_1 can be calculated using the following equations:

$$\varepsilon_1 = \ln \frac{b}{d} \quad \ldots\ldots\ldots\ldots \quad (3a)$$

$$\delta_1 = \ln \frac{A_o}{A} \quad \ldots\ldots\ldots\ldots \quad (3b)$$

In the case where υ is constant and then $\delta_1 = f(\varepsilon_1)$ the following equation can be obtained:

$$\delta_1 = \frac{1}{\upsilon} \varepsilon_1 + \delta_n \quad \ldots\ldots\ldots\ldots \quad (4a)$$

or after transformation

$$b = d \exp[\nu(\delta_1 - \delta_n)]$$

During deformation the length of the voids formed, becomes equal to the interparticle spacing. At this point, shear between the voids occurs, followed by their coalescence (11).

The void growth model described by equation 4b is used to discuss the results of this investigation.

EXPERIMENTAL PROCEDURE AND RESULTS

The chemical composition in wt% of the steel used in this study is shown in Table I.

TABLE 1 - Chemical composition in wt% of the steel used.

C	Mn	P	S	Si	Cu	Cr	Mo	Al	Sn	N_2
0.32	0.90	.010	.019	0.22	.11	0.82	0.17	.015	.014	.015

The as received material was a 200mm x 200mm x 500mm piece from the original continuously cast slab. A 12.5mm slice of this material was cut, machined and etched to obtain the general solidification and segregation structures. Detailed optical and scanning electron microscopy were conducted to characterize the nature, morphology and distribution of the non-metallic inclusions present in this steel. The results are shown in figures 1 and 2. The microscopic results from figure 1 indicated that the nonmetallic inclusions were manganese sulfides (figure 1e). In addition, the results from figure 2, corresponding to stereological measurements of the morphology of inclusions in both the columnar (zone A) and equiaxed (zone B) regions, revealed an interesting point. The inclusions observed and measured in the equiaxed zone were more elongated and numerous than the inclusions observed in the columnar zone (compare figures 1b and 1d versus 1d and c). The fact that the inclusions observed in the equiaxed zone have a larger shape factor $\lambda = 1/d$ than the inclusions located in the columnar zone was to some extent unexpected.

Prior to the determination of the hot ductility of this steel, a series of reheating studies were conducted to determine the austenite grain size at various temperatures. Samples from different positions of the slab (below the original cast surface, quarter

point (columnar zone A), center (equiaxed zone B) were used in the reheating studies. The results of the austenite grain size versus reheating temperature for two positions are shown in figure 3. Once the grain coarsening temperature (T_{GC}) was established, the hot ductility tests were conducted below the T_{GC}<1480K. This was done to isolate the contribution of austenite grain size to hot ductility.

To measure the hot ductility of the steel, hot compression tests, were carried out as a function of determation temperature and constant strain rate. Flanged samples (7) from the columnar and equiaxed zones, with the deformation axes parallel to the solidification direction were machined. The tests were conducted in a modified high temperature - computer controlled MTS-252 machine. The flanged samples were placed inside of the furnace chamber, heated to 1480K, held for 2 minutes and then cooled down to the desired deformation temperatures. The range of deformation temperatures was between 1273K and 1473K. All the samples were deformed at a constant strain rate of 5.0 sec^{-1}. The experimental procedure to determine the forming limit diagram is described elsewhere (7). The results from the hot ductility determinations are illustrated in figures 5a through 5d. The slope of the fracture lines obtained in this investigation are in good agreement with Kuhn's experiments (7). In addition to the above experiments, studies to compare the fundamental micromechanisms of the fracture behavior of this steel at high and low temperature were conducted. Flat, one side polished tensile specimens from both columnar and equiaxed zones were prepared. High temperature tensile tests under vacuum conditions were conducted The experimental set-up is shown in figure 6. Also, in-situ room temperature tensile tests inside the chamber of a 700-AMR scanning electron microscope (SEM) were performed. After fracture, both high and low temperature tensile specimens were observed under the optical and SEM microscopes. Typical results of these observations are shown in figures 7a through 7f. During the in-situ tensile tests the increase of void size was measured. The void growth ratio (υ) as a function of inclusion morphology was calculated and the results are presented in figure 4.

DISCUSSION

The hot ductility results obtained in this investigation (figures 5a - d) can be clearly explained in terms of the morphology and distribution of the non-metallic inclusions present in the steel. For example, in the columnar zone (zone A) near to the equiaxed zone (zone B) the non-metallic inclusions have a shape factor (λ) of about 2.4. In the equiaxed zone the inclusions have a λ of about 5.6. These differences in morphology and distribution of non-metallic inclusions in both the columnar and equiaxed zone can be seen in figures 1a-d and 2a,b. In addition, as expected, the hot ductility of the steel was strongly related to the

deformation temperature for a given inclusion morphology and distribution (see figures 5a-d). From these figures it can be seen that the position of the fracture line, as defined by the construction of the forming limit diagram, decreases with deformation temperature. The decrease in the position of the fracture line was larger for samples containing non-metallic inclusions with $\lambda > 5.0$. The fracture lines shown in figures 5a,b,d have a equation of the type $\delta_{1F} = C - \frac{1}{2}\,\delta_{2F}$. This line can be used as the hot ductility criterion for this steel. For example, deformations above this line will result in fracture, while deformations below the fracture line will be free of fracture for a given set of high temperature deformation conditions.

Optical and scanning electron microscopy of the compression and tensile samples used in this study revealed that nucleation of voids took place at early stages of plastic deformation (e.g. in the range 1 to 5 percent of the total deformation, δ_{1F}). The above was observed for all experimental temperatures used. After nucleation of voids, the stable void growth stage in the vicinity of the inclusions was observed. Typical examples are shown in figures 7a, b. The next stage, void coalescence, appears to occur via different mechanisms at room temperature and at high temperature. That is, the void coalescence that took place at room temperature occurred by a shear mechanism - figure 7d . The void coalescence of the second phase particles that took place at high temperatures occurred via two mechanisms. The first one was the plastic rupture of the matrix (figure 7e). The second one was the coalescence of voids by intergranular cracks (figures 7f). The mechanism of void coalescence illustrated in figures 7c and f was preferentially observed as the deformation temperature increased (1273K to 1473K). A possible explanation of the aforementioned behavior could be connected with segregation of tramp elements (e.g. P, As, Sb, and Sn) to the prior γ grain boundaries.

The quantitative measurement of the void growth process - $\upsilon = f(\lambda, T)$ are shown in figure 4. The results from figure 4 revealed that the void growth ratio, υ, increases as λ increases. Similar trends were observed at both room and high temperature. However, υ increases at smaller ratio at high temperatures than at low temperatures. The changes in the fracture behavior of the steel in terms of inclusion morphology and testing temperature can be explained using the experimental results illustrated in figure 4 and the data obtained from equation 4b. That is, for a given deformation temperature and void growth ratio, a plot, mean length of voids , b, versus the true tensile strain of sample , δ_1, can be constructed , $b = f(\delta_1)$. This type of plot is shown in figure 8. In general, the plot shown in figure 8, illustrates that for a given υ, λ and deformation temperature, a family of lines $b = f(\delta_1)$ with different slopes can be constructed. Hence, for very elongated inclusions, the true tensile strain to fracture, δ_{1F}, would

be less than for inclusions with shape factor close to unity.

The simple approach described in this paper to measure and to explain the hot ductility of a steel in terms of the morphology distribution of the non-metallic inclusions and deformation temperature, is a preliminary attempt to find a quantitative treatment of the hot ductility of steels. It is well recognized, that this problem is a complex one and needs further investigation.

CONCLUSIONS

1) Hot ductility of steel strongly depends on solidification structure and segregation.

2) The void growth ratio parameter can be used to quantitatively describe the effect of morphology of non-metallic inclusions on the void growth process during ductile fracture of steels.

SYMBOLS USED

A_o = area of sample before testing (μm^2)

A = area of sample after testing (μm^2)

b = mean void size (μm)

b_F^H = critical void size at high temperature (μm)

b_F^R = critical void size at room temperature (μm)

d = mean inclusion diameter (μm)

l = mean inclusion length (μm)

n = number of particles measured

N_A = number of particles per unit area (mm^{-2})

T_{GC} = austenite grain coarsening temperature (K)

$d\delta_1$ = differential of the mean true strain of sample

δ_1 = mean true strain of sample

δ_{1F} = critical strain of sample

δ_n = true strain of sample necessary to nucleate voids

δ_2 = compressive true strain of sample

$d\varepsilon_1$ = differential of the mean true strain of voids

ε_1 = mean true strain of voids

σ = standard deviation

λ = inclusion shape factor

υ = void growth ratio

$\Delta H/H$ = height reduction of flanged sample (%).

REFERENCES

(1) Lankford, W.T., Metall. Trans., vol. 3, 1972 pp. 1331-1357.

(2) Baker, T. J., and Johnson, R., J. Iron and Steel Inst., vol. 211, 1973, pp. 783-791.

(3) Sellars, C. M., and Tegart, McG., Int. Metall. Rev., vol. 17, 1972, pp. 1-24.

(4) Tegart, McG., "Ductility," Metals Park, Ohio, ASM, 1968.

(5) Moore, P., "Deformation Under Hot Working Condition," The Iron and Steel Institute, London, 1968.

(6) McQueen, H. J., and Jonas, J.J., "Metalforming: Interrelation Between Theory and Practice," edited A.L. Hoffmanner, Plenum Press, New York, 1971.

(7) Kuhn, H.A., Formability Topics - Metallic Materials, ASTM STP, 647, 1978, pp. 206-219.

(8) Gurland, J., and Plateau, J., Trans. ASM, vol. 56, pp. 442.

(9) Argon, A.S., JM, J., and Sagoflu, R., Metall. Trans., vol. 6A, 1975, pp. 825.

(10) Pytel, S., and Rudnik, S., Archiv. Hutn., vol. 24, 1979, pp. 58.

(11) Brown, L.M., and Embury, J.D., "The Microstucture and design of Alloys", the Institute of Metals and the Iron and Steel, London, 1973.

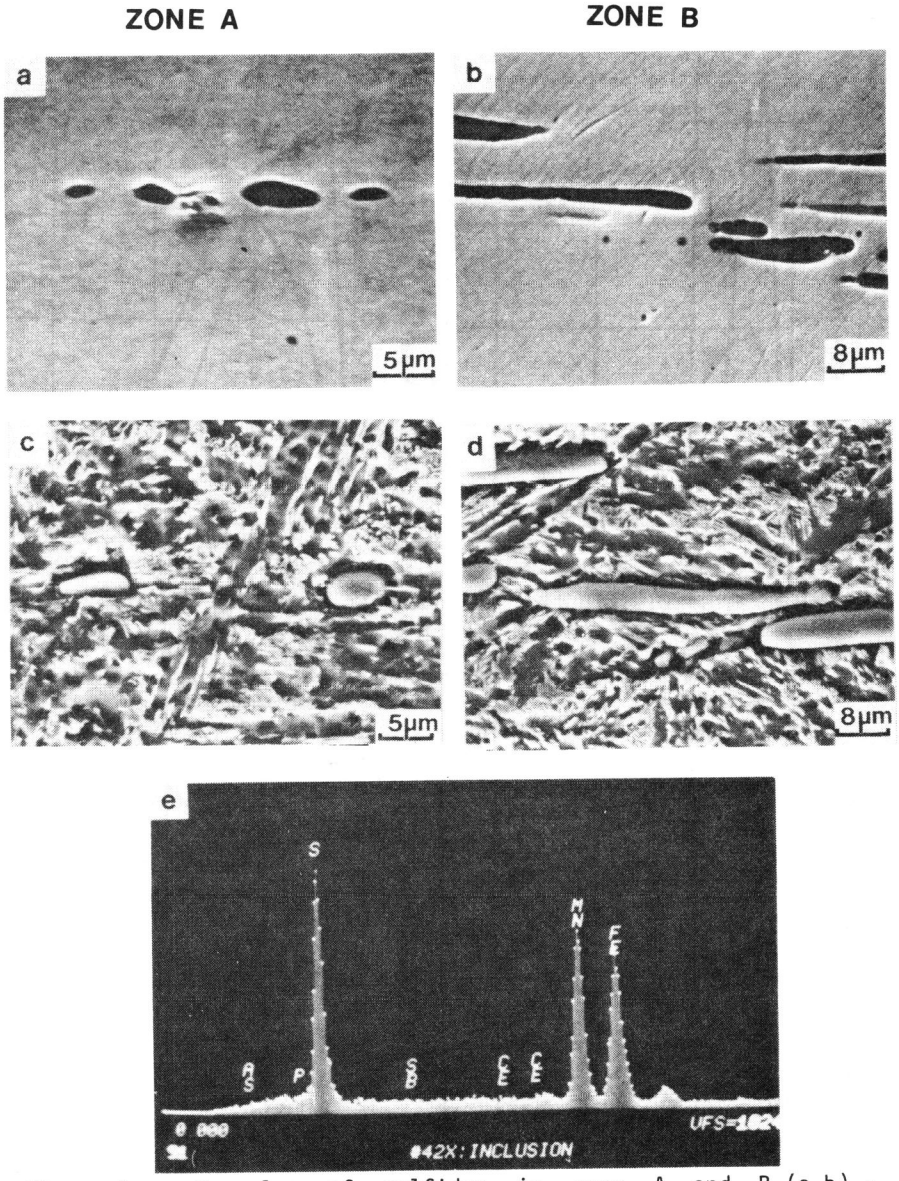

Figure 1a-e. Examples of sulfides in zone A and B,(a,b) - Typical inclusion shape without etching (c,d) - after deep etching, (3) Energy disperse spectrometry of inclusions.

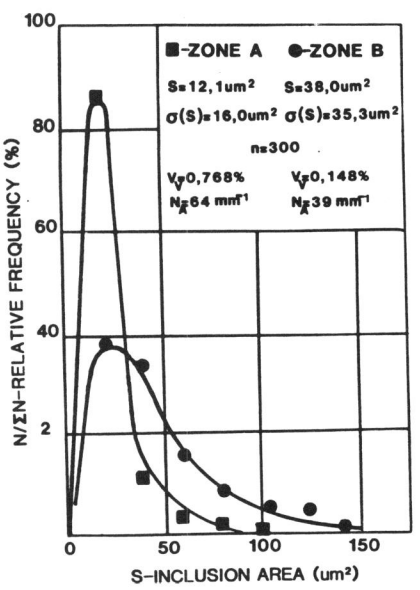

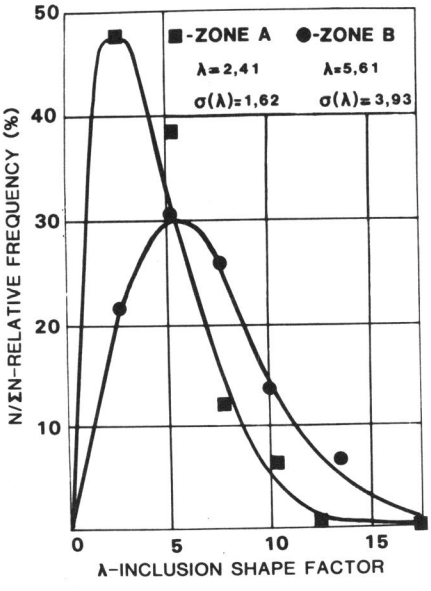

Figure 2a,b. Distribution of inclusion area (2a) and inclusion shape factor (2b) for both zones tested.

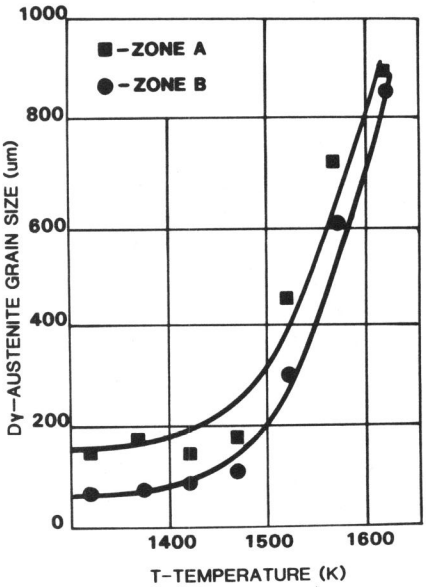

Figure 3. Results of austenite grain coarsening studies.

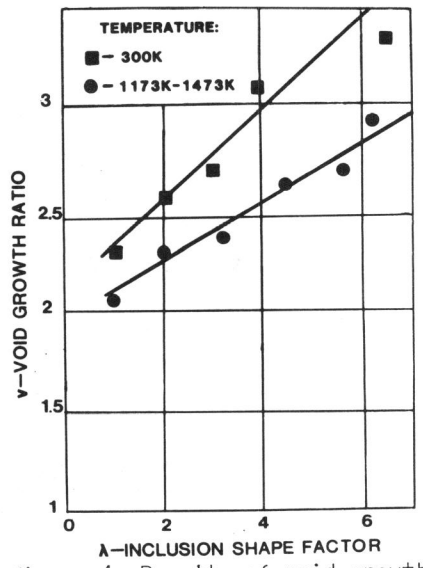

Figure 4. Results of void growth ratio measurements.

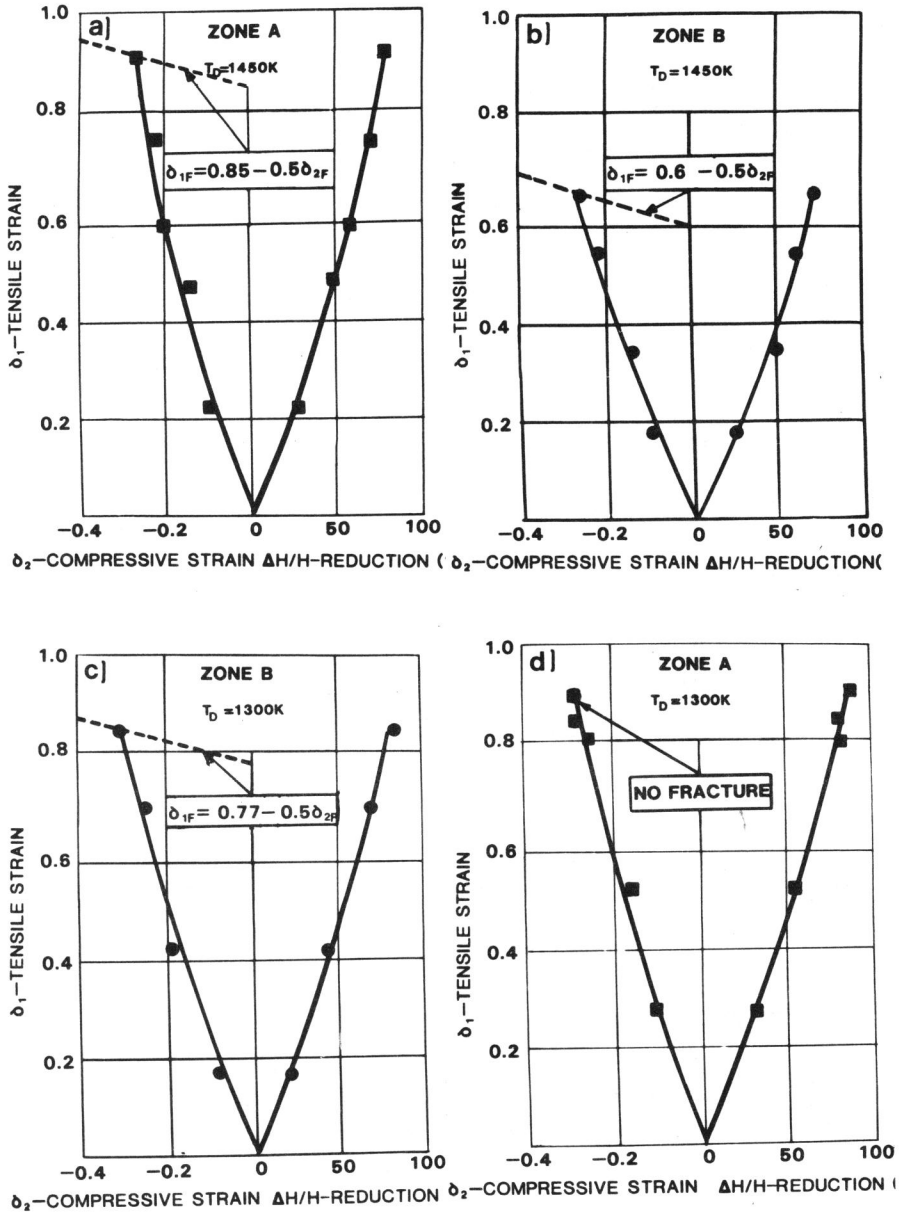

Figure 5a-d. Effect of deformation temperature and zone tested on the hot ductility of flanged samples.

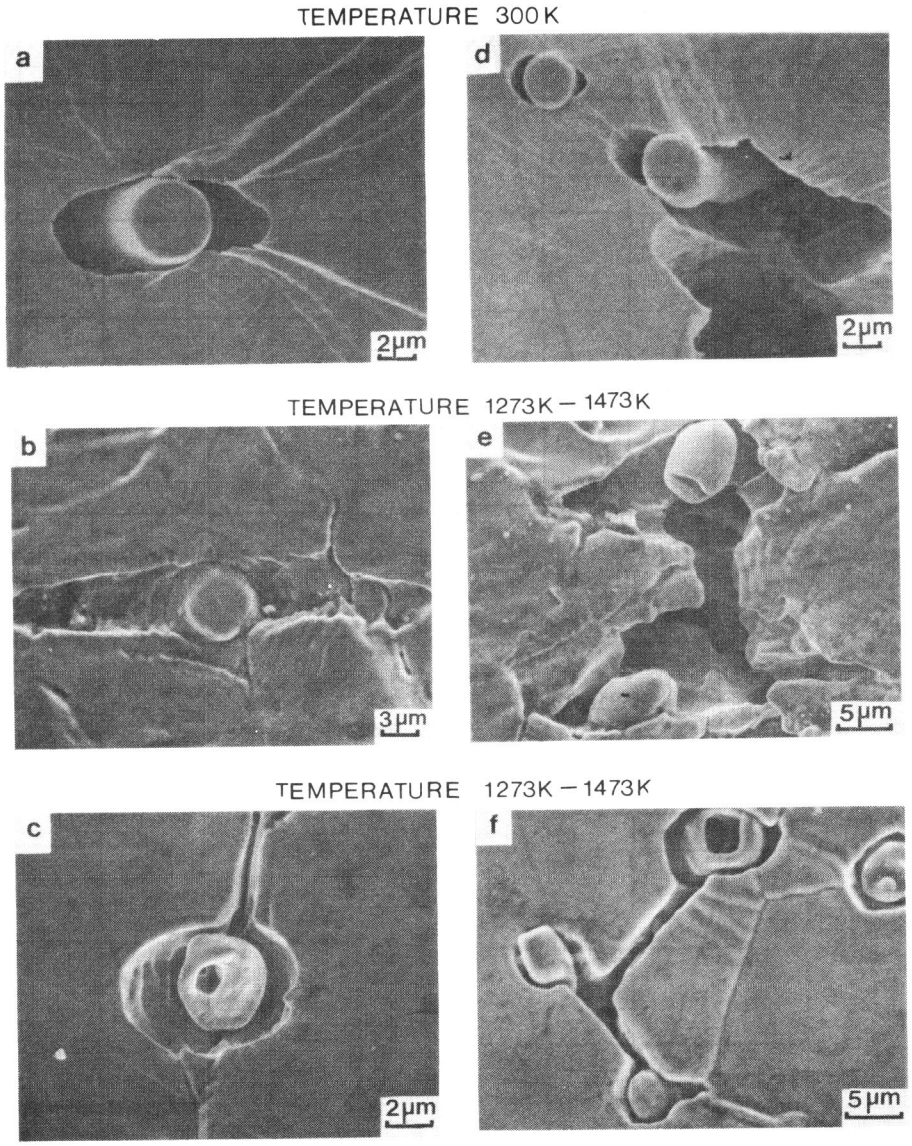

Figure 7a-f. Examples of nucleation, growth, (a,b,c) and coalescence of voids and microcracks (d,e,f) in vicinity of sulfides

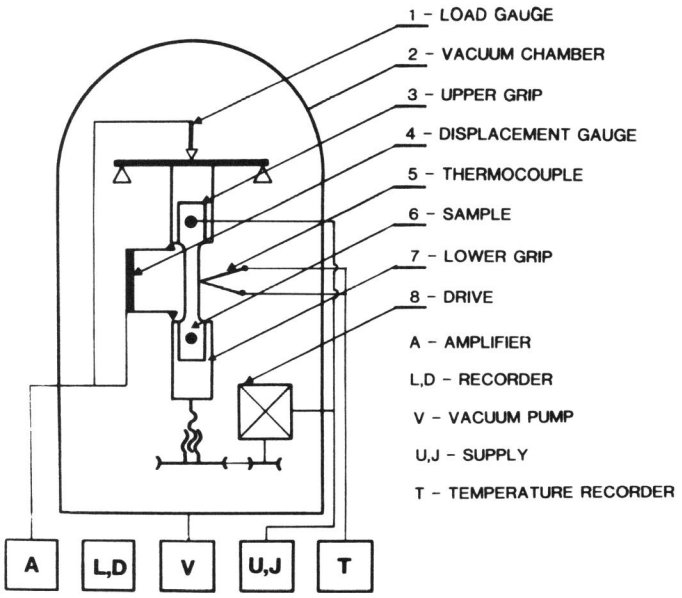

Figure 6. Equipment for tensile tests at high temperature.

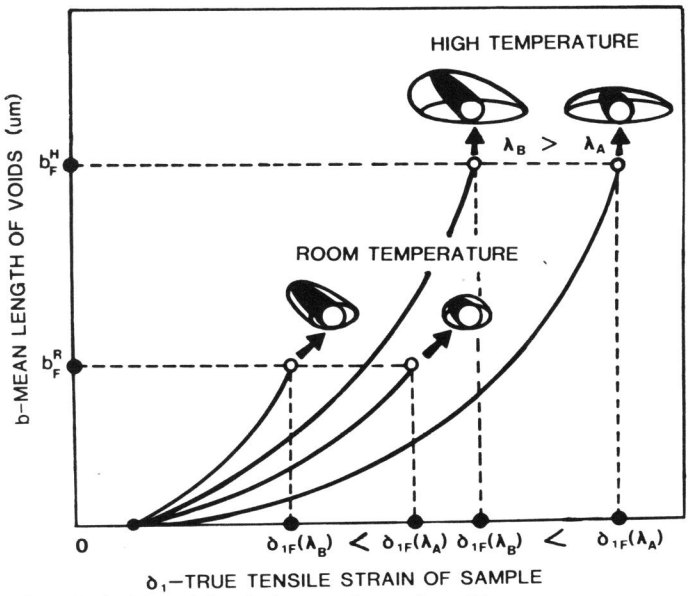

Figure 8. Relationship between true tensile strain of sample and mean length of voids.